Ground state and thermal properties of a lattice gas on a cylindrical surface

M. Mercedes Calbi,[1] Silvina M. Gatica,[1,2] Mary J. Bojan,[3] and Milton W. Cole[1]
[1]*Department of Physics, Pennsylvania State University, University Park, Pennsylvania 16802*
[2]*Departamento de Física, Universidad de Buenos Aires, and CONICET, Buenos Aires 1428, Argentina*
[3]*Department of Chemistry, Pennsylvania State University, University Park, Pennsylvania 16802*
(Received 6 September 2002; published 30 December 2002)

Adsorbed gases within, or outside of, carbon nanotubes may be analyzed with an approximate model of adsorption on lattice sites situated on a cylindrical surface. Using this model, the ground state energies of alternative lattice structures are calculated, assuming Lennard-Jones pair interactions between the particles. The resulting energy and equilibrium structure are nonanalytic functions of radius (R) because of commensuration effects associated with the cylindrical geometry. Specifically, as R varies, structural transitions occur between configurations differing in the ''ring number,'' defined as the number of atoms located at a common value of the longitudinal coordinate (z). The thermodynamic behavior of this system is evaluated at finite temperatures, using a Hamiltonian with nearest-neighbor interactions. The resulting specific heat bears a qualitative resemblance to that of the one-dimensional Ising model.

DOI: 10.1103/PhysRevE.66.061107 PACS number(s): 68.60.−p, 64.70.−p, 68.43.−h, 67.70.+n

I. INTRODUCTION

Atoms or molecules may be confined either within, or on the outside surface of, cylindrical materials, such as carbon nanotubes. The existence of such systems raises a set of interesting questions concerning the thermal, structural, and dynamical properties of a cylindrical monolayer film. In this paper, we evaluate the thermal and structural properties of such a film, with the help of two simplified models. We believe that some of our results are realistic, although others may be artifacts of the model [1,2]. For example, Fig. 1, taken from a previous work [2], depicts the density of H_2 molecules within a nanotube of radius $R=7$ Å, at temperature $T=10$ K. Note that the radial spread of the so-called ''cylindrical shell'' phase is some 10% of the mean radial distance $\langle r\rangle \approx 3.8$ Å. In such a situation, the model of confinement to a precise value of R would seem appropriate.

The first task we undertake is to ascertain the ground state energy and structure of an ensemble of atoms, assumed to be classical, that interact with all other atoms with a Lennard-Jones (LJ) pair potential: $U(r)=4\epsilon[(\sigma/r)^{12}-(\sigma/r)^6]$. Here σ is the nominal diameter of the atoms and ϵ is the well depth of their mutual interaction. We assume, without proof, that the equilibrium structure is a periodic crystal. To determine its properties, we minimize the ground state energy per particle in this cylindrical surface lattice. In so doing, we consider possible periodic structures and determine that structure which has the lowest energy at any specified value of R. The second problem is to evaluate the thermal properties of such a ''lattice gas'' which has varying fractional site occupancy θ. In this case, we simplify the problem by including just nearest-neighbor interactions.

The behavior of the system can be expressed in terms of a reduced radius $R^*=R/\sigma$. Both the ground state and finite temperature (T) problems have much-studied one-dimensional (1D) and 2D limits, corresponding to $R^*=0$ and ∞, respectively. Interestingly, the behavior does not interpolate smoothly between these limits as R^* is varied. This happens because [3] of a commensuration effect arising from the periodicity associated with the azimuthal angle ϕ. This phenomenon is analogous to that found in monolayer films in the regime where the film's lattice constant is similar to that of the substrate [4]. In the cylindrical case, the circumference of the cylinder provides the length scale that determines the compatibility of candidate structures. While there have been many studies of adsorption within nanotubes [5], we believe that this represents the first detailed exploration of the problem of the radius dependence of the low-temperature thermodynamic properties of films adsorbed in the inner wall (cylindrical shell) phase. As such, our predictions of thermal properties, will be relevant to future experimental studies.

In the following section, we evaluate the ground state problem by considering a rather general set of alternative structures. In Sec. III, we compute the specific heat for sev-

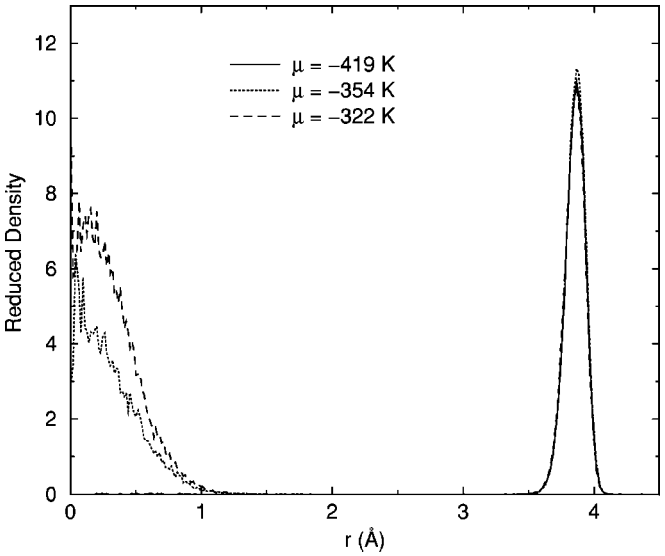

FIG. 1. Reduced density $\rho^*=\rho\sigma^3$ of H_2 molecules at $T=10$ K as a function of radial distance inside a nanotube of radius 7 Å for several values of the chemical potential μ (taken from Ref. [2]).

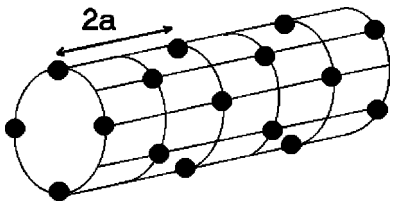

FIG. 2. Schematic depiction of the cylindrical lattice structure having ring number $\nu=4$. The lattice constant is $2a$.

eral values of the ring number. Finally, in Sec. IV we estimate the quantum effects (by including zero-point energy) present in a rather extreme case, ^{4}He atoms on a cylindrical surface, and compare the resulting energy with the known energy.

II. GROUND STATE ENERGY

We assume that the ground state structure is close packed, as exemplified in Fig. 2, and that it can be derived with the following algorithm. At any specific value, say zero, of the coordinate (z) parallel to the cylinder's axis, there are ν atoms, distributed uniformly in azimuthal angle ϕ. We call ν the ring number of the structure and consider structures with integral value of ν. Figure 2 depicts the case $\nu=4$, which turns out to be an important example. A unit cell of this structure consists of four atoms at $z=0$ (at azimuthal angles $\phi=0$, $\pi/2$, π, and $3\pi/2$) and four atoms at $z=a$ ($\phi=\pi/4$, $3\pi/4$, $5\pi/4$, and $7\pi/4$). The structure is characterized by a one-dimensional density $\rho=4/a$, since there are eight atoms in a unit cell of length $2a$. For each such hypothetical structure, we have performed two calculations. The first is a total energy calculation, aimed at determining the lowest energy structure. The energy in this case is taken as the sum of two-body LJ interactions between atoms at all lattice sites. The second study yields the thermodynamic properties, described in the following section.

Before embarking on these calculations, we assess the models. The only approximations in the ground state calculation are the use of Lennard-Jones potentials, the omission of kinetic energy, and the assumption that the actual structure fits the close-packing description. The first two are conventional approximations in the lattice gas approach. We note only that many-body corrections may be important in this geometry (but we ignore them) [6]. The third assumption seems logical, since all simple close-packed lattice structures are included. One can imagine other possibilities, such as one in which the unit cell consists of more than two rings, but these seem implausible to us. We note that the problem of packing on a spherical surface is quite different from that on a cylinder; there, frustration arises because of the difficulty of satisfying local packing requirements [7,8]. Here, instead, we find many high density, strongly bound, and nearly degenerate low-energy structures, which do satisfy local bonding requirements.

We have obtained the (ground state) energy results from the following procedure. For any assumed values of the ring number and cylinder radius, the energy $E_\nu(a,R)$ is evaluated by summing contributions from all interatomic interactions,

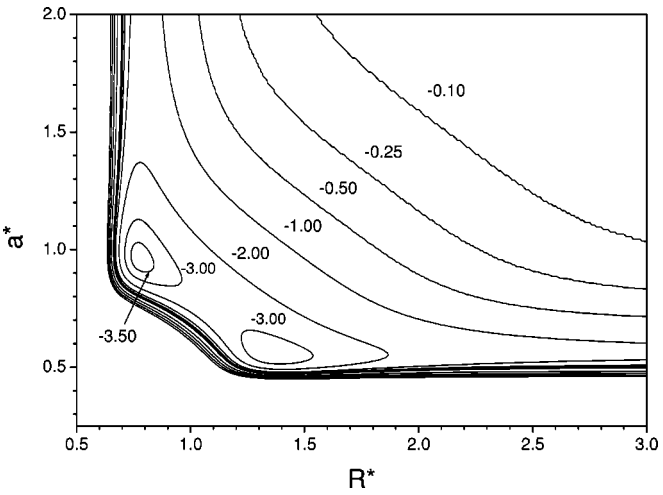

FIG. 3. The energy per particle $E_\nu(a^*,R^*)/(N\epsilon)$ is shown for the case $\nu=4$, as a function of the ring separation $a^*=a/\sigma$ and radius $R^*=R/\sigma$.

$$E_\nu(a,R)=\sum_{i<j} U(r_{ij}). \tag{1}$$

Here, the sum includes all pairs of atoms, separated by a 3D distance r_{ij}. It is convenient to measure distances in units of the hard core parameter, to permit scaling between different solutions. Thus, R^* and $a^*=a/\sigma$ are reduced distance variables; similarly $E^*=E/\epsilon$ is a reduced energy. As an example ($\nu=4$) revealing the energy's dependence on these lengths, a contour plot of the function $E_4(a^*,R^*)$ is shown in Fig. 3. Note that this function possesses two local minima; these correspond to two quite distinct geometries. The minimum with the larger value of a^* (smaller value of R^*) corresponds to neighbors within the same ring that are separated by $\Delta r\approx r_{min}$ (the equilibrium distance of the pair potential). The other minimum energy configuration (larger value of R^*) involves nearest neighbors in adjacent rings, separated by $\Delta r\approx r_{min}$ [9]. While, in either case, the low energy of the structure comes primarily from such optimization of nearest-neighbor distances, longer range interactions do play a significant role in determining the total energy. This is evident from the fact that the (reduced) cohesive energy per particle has a maximum value as high as 3.62 for $\nu=4$. This is 45% greater than the value (5/2 for $\nu=4$) that would result if only nearest-neighbor interactions were included.

For each pair of values of ν and R, one thus determines a unique value a^*_{min} for which this energy function is a global minimum. This optimized value of a^*_{min} appears in the lower panel of Fig. 4 and the corresponding energy appears in the upper panel. In the latter, one observes two alternative behaviors: either a single value of R yields a minimum in this function (for $\nu=1$ or 2) or two values yield local minima (for $\nu>2$). In the latter case, with the single exception of $\nu=3$, the lower energy structure is the one with the smaller value of R, i.e., the case with nearest neighbors in the same ring.

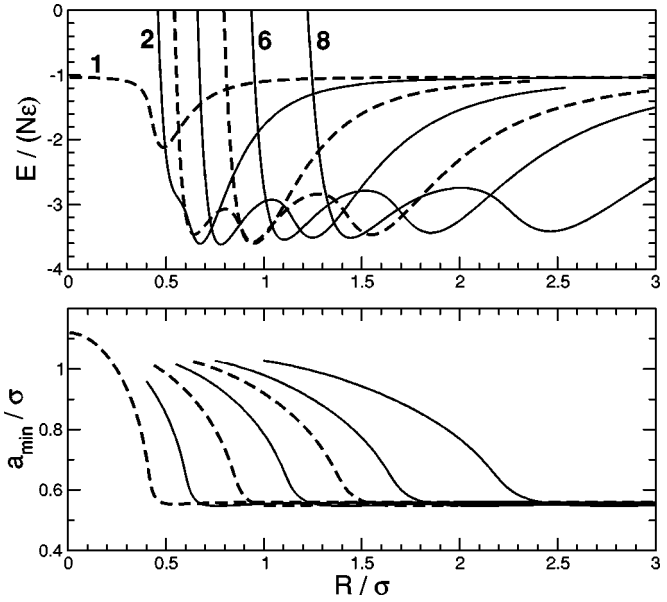

FIG. 4. Upper panel shows the energy per particle (in units of the pair potential's well depth) as a function of reduced radius, for various assumed ring numbers, $\nu=1$, 2, 3, 4, 5, 6, and 8, from left to right. Each value of E is derived by choosing the optimized lattice constant (a_{min}), shown in the lower panel. The odd ν curves are dashed and $\nu=1$, 2, 6, and 8 are labeled.

By such an analysis, we derive the ground state energy, shown in Fig. 5, representing the global lower bound of the ensemble of curves in Fig. 4. This scallop-shell-like function manifests the following plausible behavior. For very small R^*, the lowest solution corresponds to the case $\nu=1$. Near $R^*=0.5$, the lowest energy shifts to the $\nu=2$ structure; this is a plausible result because then two atoms may occupy the same ring without significant hard core repulsion. For increasing R, the minimum energy and structure undergo a sequence of transitions between different values of ν. Interestingly, the sequence is not monotonic: after a very narrow region ($0.60<R^*<0.63$) in which $\nu=3$ is optimal, there occurs a region ($0.63<R^*<0.73$) in which $\nu=2$ is optimal,

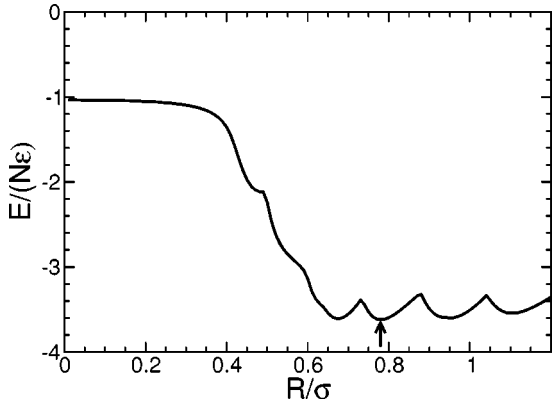

FIG. 5. Energy as a function of radius, obtained by selecting the minimum energy from the solutions in Fig. 4. The global minimum energy for this problem occurs at $R^*=0.78$ ($\nu=4$), as indicated by the arrow.

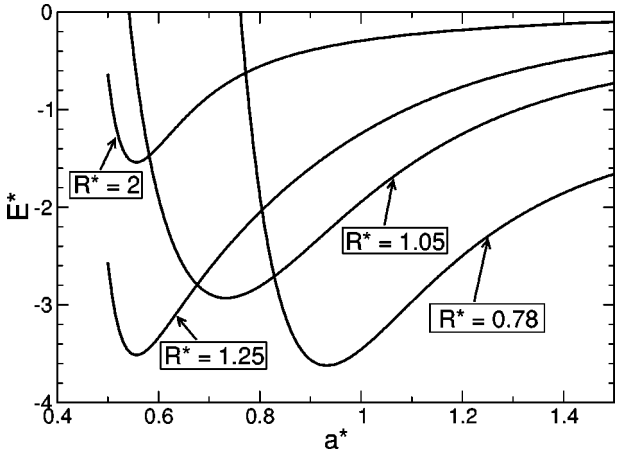

FIG. 6. Energy as a function of a^* for various values of R^* in the case $\nu=4$, see Fig. 3. The curve corresponding to $R^*=0.78$ yields the global energy minimum of the problem.

followed by an extended region ($0.73<R^*<0.87$) in which $\nu=4$ provides the lowest energy. Note that there are many energy minima close to the (reduced) energy $E/(N\epsilon)=-3.6$. The global minimum energy structure occurs at $R^*=0.78$, with reduced energy -3.62 (the minimum near $R^*=0.67$ has energy -3.61 and that near $R^*=0.95$ has energy -3.60). At that point, there are two neighbors at reduced distance 1.10 and four at distance 1.11, both of which are very close to the pair potential minimum value, $r^*_{min}\approx 1.12$. This most cohesive configuration corresponds to a cohesive energy some 7% higher than the two-dimensional ground state energy (3.38) of the L J potential (corresponding to a hexagonal packing) [10]. This result implies that if atoms were to self-assemble on a surface of any shape, the cylindrical surface would be stable relative to the planar surface. While we have not performed the corresponding calculation for atoms on a spherical surface, we suspect that the energy in that case would be competitive with the present results [11]. Based on experience found in the case of a Coulomb interaction [7,8], we expect that frustration due to many energetically similar structures would be likely to occur in the spherical case. We note, for completeness, that the reduced cohesive energy in 1D is slightly greater than 1 (1.03), while in 3D the value is quite large (8.1), a result of both the higher coordination possible in 3D and the large contribution of long range forces.

A structure of the type we are studying will sustain sound waves with various polarizations. The simplest such wave is a longitudinal compressional wave, with propagation vector parallel to the cylinder's axis. In the long wavelength limit, the corresponding sound speed for the case of mass M particles will satisfy

$$Ms^2=a^2\left(\frac{\partial^2(E/N)}{\partial a^2}\right)_R . \tag{2}$$

Here the derivative is evaluated at the ground state configuration for any R. Figure 6 shows corresponding energy curves from which the derivatives in Eq. (2) may be com-

puted. For the curves shown, the reduced sound speed Ms^2/ϵ has the values 86, 37, and 91 at $R^*=0.78$, 1.05, and 1.25 (the three lowest energy minima in Fig. 6), respectively. In the case of a mass 16 particle (CH_4), these values correspond to $s\approx 3$ km/s, comparable to the bulk speed of sound of CH_4. The very high value is indicative of a very tightly bound and rigid structure.

III. THERMODYNAMICS

There exists a venerable tradition of applying the (Ising) lattice gas model to describe the condensation of gases. The critical exponents of the liquid-vapor transition are believed to be exactly determined with this model. As is common in such applications, we simplify our calculations by assuming that only nearest neighbors interact and these interactions all have the same energy ($-J$). While J might simply be set equal to the well depth of the pair potential, a more sophisticated model might increase the value of J to incorporate attractive, longer range interactions in some approximation. The preceding section's results for the energy would suggest that an increase of J/ϵ by a factor ~ 1.5 is needed to derive the ground state's energy. However, at a density less than complete filling of sites, the occupation fraction would reduce this hypothetical long range correction significantly. Of course, accurate calculations (not undertaken here) would incorporate longer range interactions explicitly in the Hamiltonian itself.

Our method of study is the explicit evaluation of the partition function, within the canonical ensemble. For the case when N sites are occupied at temperature T, this function is

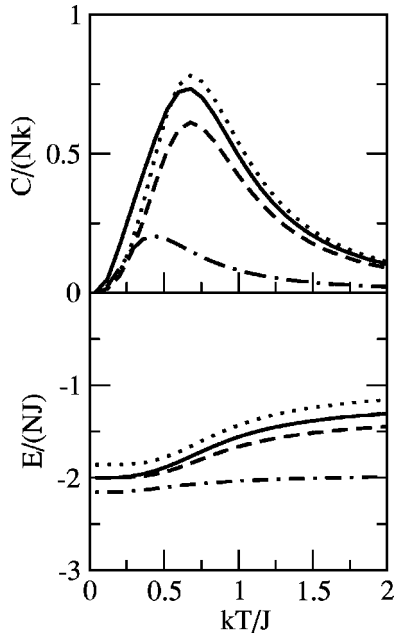

FIG. 7. Energy (lower panel) and specific heat (upper panel) for the case of ring number $\nu=2$, $N_s=16$ (eight rings). The full curve corresponds to half filling occupancy ($\theta=8/16$), the dotted curve to $\theta=7/16$, the dashed one to $\theta=9/16$, and the dot-dashed one to $\theta=13/16$.

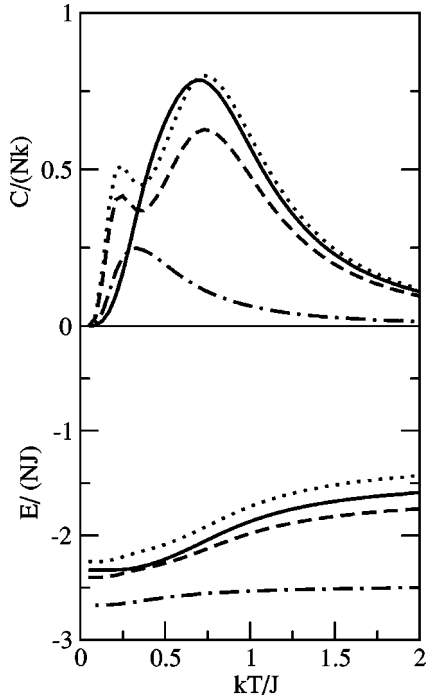

FIG. 8. Energy (lower panel) and specific heat (upper panel) for the case of ring number $\nu=3$, $N_s=18$ (six rings). The full curve corresponds to half filling occupancy ($\theta=9/18$), the dotted curve to $\theta=8/18$, the dashed one to $\theta=10/18$, and the dot-dashed one to $\theta=15/18$.

$$Q_N(T)=\sum e^{-E\{n_i\}/kT}. \tag{3}$$

Here, k is the Boltzmann's constant, the sum is over all configurations $\{n_i\}$ that yield a total of N particles (out of N_s sites), and $E\{n_i\}$ is the corresponding energy. Each configuration corresponds to a specific choice of occupied sites. Periodic boundary conditions are employed, so that the right end sites of a periodic region interact with ''neighboring'' left end sites of that region. A typical calculation involves a configuration determined by the occupancy of the 6ν sites contained within three unit cells of the lattice. We explore the accuracy of this procedure by varying the size of the periodic cell. Because there is no transition in this 1D system, the finite size effects do not attenuate any divergence in the specific heat, but they are observable. Checks on the results come from the known ground state energy and the high T energy, obtained from a random site occupancy,

$$E/(NJ)=-\frac{\gamma}{2}\frac{N}{N_s}=-\frac{\gamma}{2}\theta. \tag{4}$$

Here γ is the coordination number and θ is the occupied fraction of sites. Another check comes from the entropy $S(T)$, which is obtained by integrating the heat capacity, divided by T, from zero to infinity, where $S=\ln\{N_s!/[N!(N_s-N)!]\}$. Note that $S/N_s=-\theta\ln\theta-(1-\theta)\ln(1-\theta)$, i.e., ln 2 at 50% occupancy.

Figures 7–9 show the energy and specific heat as functions of the reduced temperature $T^*=kT/J$ for the cases ν

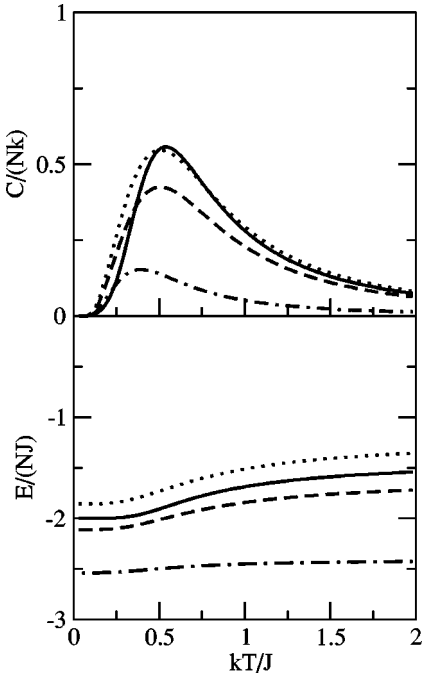

FIG. 9. Energy (lower panel) and specific heat for the case of ring number $\nu=4$, $N_s=16$ (four rings). The full curve corresponds to half filling occupancy ($\theta=8/16$), the dotted curve to $\theta=7/16$, the dashed one to $\theta=9/16$, and the dot-dashed one to $\theta=13/16$.

$=2$, 3, and 4, respectively. We make a number of remarks about the results. First, the curves are all qualitatively similar; this is not surprising because none of these finite ν cases exhibits a phase transition. Hence, all of the interesting behavior is concentrated in the regime near and below $T^*=1$. The key qualitative dependence is a concentration, with increasing ν of the thermal ''activity'' into a progressively narrower region of T. This trend is plausible because the limit of very large ν is the (triangular lattice) 2D limit, which exhibits a genuine phase transition, with critical temperature $T_c^*\approx 0.91$.

Size effects are present in our calculations and may also occur in nature, where nanotubes are finite or may have finite segments that are perfectly ordered. To explore these effects, we focus on the case $\nu=3$. Figure 10 shows how the ground state energy (inset in left panel), at $\theta=1/2$, depends on N_s, the number of sites in the unit cell, while the high T result remains fixed at $E/(NJ)=-3/2$, the exact result at high T arising from the 50% site occupancy. The dependence on N_s for $\theta=1/2$ conforms to the expression $E(T=0)/(-NJ)=3-12/N_s$, derived from the bulk and surface energies of a ground state ''island'' consisting of $N_s/6$ isolated rings. Hence, the largest system shown ($N_s=30$) has a ground state energy differing from the infinite system result by a fraction $4/30\approx 0.14$. The specific heat bump moves to progressively higher T as N_s increases; it is seen to be converging to a well defined limit at that point, with a maximum near $T^*=0.89$, as is expected from the limiting behavior described above.

One particularly interesting feature is the presence of a double maximum in the specific heat at fractional occupations θ both near, but not equal to, 1/2 (Fig. 10, right panel).

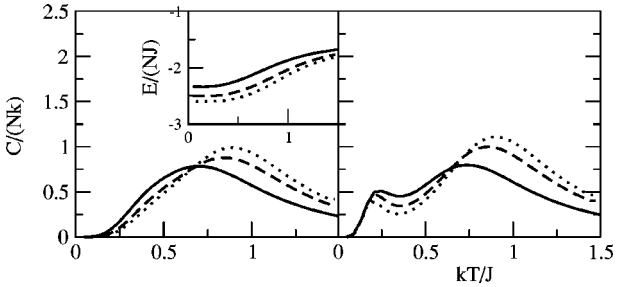

FIG. 10. Specific heat for $\nu=3$, showing the size effect as the number of sites N_s increases. The full curve depicts the case for $N_s=18$ (six rings), the dashed curve corresponds to $N_s=24$ (eight rings), and the dotted curve to $N_s=30$ (ten rings). The left panel shows the case for half occupancy (the inset depicts the energy per particle) whereas the right panel corresponds to occupancy below 1/2: $\theta=0.44$ (full curve), 0.42 (dashed curve), 0.43 (dotted curve).

Note that this behavior becomes increasingly evident as the system size grows, indicating that it is not a finite size artifact. To explore this phenomenon, we compute two correlation functions, defined in the following way. The transverse correlation function is obtained from the average of the product of the occupation numbers of the three sites in the same ring, and the longitudinal correlation function is the average of the product of the occupation numbers of three sites in consecutive rings.

These correlation functions are plotted in Fig. 11 in the case of $\nu=3$, for the same occupations as in Fig. 8. One observes drastically different behavior for $\theta=1/2$ and $\theta\neq 1/2$. For $\theta=1/2$, there arises transverse correlation below $T^*=0.75$, persisting down to $T=0$, while the longitudinal correlations remain low and constant for the whole range of temperature. The ground state includes completely filled rings (perfect transverse order) but the longitudinal order is imperfect, e.g., because the islands have edges at $\theta=1/2$. Note that the peak in the specific heat appears at the same temperature ($T^*\approx 0.75$) for which the transverse correlations start to develop, indicating a quasitransition to a more or-

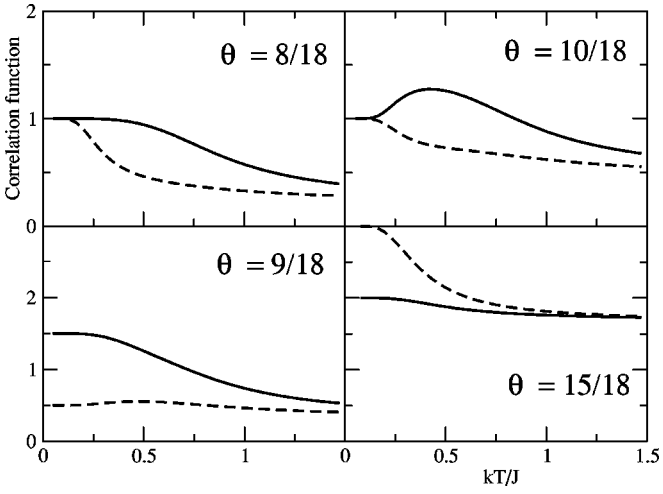

FIG. 11. Transverse (full curves) and longitudinal (dashed curves) correlation functions (defined in the text) for the same occupancies as in Fig. 8 ($\nu=3$).

dered state along the azimuthal direction.

How do we explain the second, low T, bump in C for θ close to 1/2? We attribute it to development of the longitudinal correlation at a lower T since the rings are not all complete in this case. The upper panels of Fig. 11 ($\theta=8/18$ and 10/18) show how the longitudinal correlation arises for T^* below 0.25, i.e., a much lower T than where the transverse order begins, giving rise to the corresponding low T bump in Fig. 8. Rings start to form at $T^*\approx 0.75$ and this ordering leads to a longitudinal quasicondensation when these rings start to order along the z direction as T is lowered. When the occupation is considerably larger that 1/2 (for example, as shown in the bottom right panel of Fig. 11, for $\theta=15/18$), the longitudinal order prevails because almost all the rings are occupied and the low T islands are bigger.

Based on the behavior of these two correlation functions we can also explain the absence of two peaks in the $\nu=2$ and $\nu=4$ cases. For half filling, the longitudinal order is always poor because the system tends to aggregate in an island and the peak in the specific heat corresponds to the development of the azimuthal order characteristic of this structure. For occupancy much greater than 1/2, the system tries to condense along the z direction, which coincides with the formation of a much bigger island and the specific heat peak indicates the appearence of this longitudinal order. However, because the energy difference between the transverse and longitudinally ordered structures is smaller than in the $\nu=3$ case, for intermediate cases when θ is close to 1/2, longitudinal and transverse ordering occur at nearly the same T, resulting in a single peak in the specific heat.

IV. QUANTUM EFFECTS

The preceding discussion deals with the classical lattice problem, leaving open the question of quantum effects. If one were to compute the rms fluctuations of atomic displacements due to zero-point motion, the (essentially) 1D phonon states of this lattice would lead to a divergent result. Hence, no crystalline state is possible for our lattice, even at $T=0$.

However, we wish to consider the implication of our results for the case of a rather extreme quantum problem, the ground state of ^{4}He atoms confined to a cylindrical surface. In this case, there is no ambiguity about the ground state, since it is surely a liquid, as in 3D. Our concern here is a quantitative one: what is the binding energy of this ground state? We answer this question with an estimation method similar to the one used by London more than half a century ago in describing ^{4}He in 3D [12]. The goal here is to see whether the lattice model contains any physics relevant to the ^{4}He case.

One estimate of the total energy E_{tot} of the system is the following:

$$E_{est}^{(1)}=\langle V\rangle_0+K_{est}. \tag{5}$$

Here $\langle V\rangle_0$ is the ground state energy computed in Sec. II for a cylindrical lattice. The latter is a lower bound to the true potential energy of the quantum problem. Hence, the total $E_{est}^{(1)}$ is a lower bound if the kinetic energy K_{est} were known

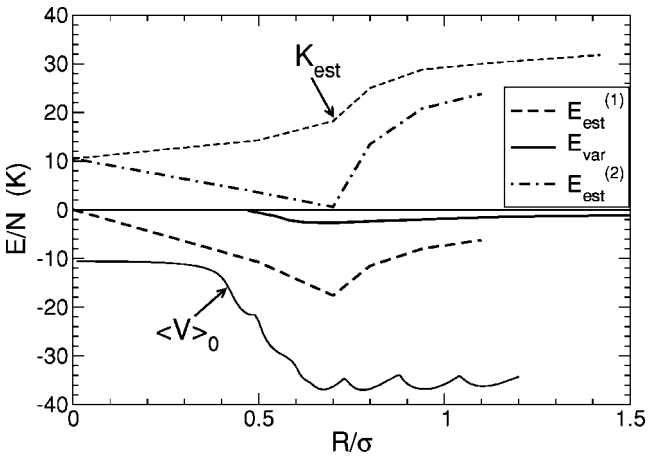

FIG. 12. The ground state energy of ^{4}He atoms confined to a cylindrical surface. The full curve shows the result of the variational calculation E_{var} by Carraro (Ref. [1]). Also shown are two alternative estimates $E_{est}^{(1)}$ and $E_{est}^{(2)}$ of the total energy obtained from the classical potential energy $\langle V\rangle_0$ and estimated kinetic energy, K_{est}, as described in the text.

to be less than, or equal to, the true kinetic energy of ^{4}He. Unfortunately, we cannot establish such a relation without carrying out a full calculation. Instead, we approximate K_{est}, following London, leading to a total energy estimate, instead of a genuine bound. Our estimate of the kinetic energy per particle includes contributions from both azimuthal and longitudinal motions for atoms within the lattice,

$$K_{est}/N=\frac{\hbar^2}{2m}\left[\left(\frac{\pi}{a}\right)^2+\left(\frac{\nu}{R}\right)^2\right]. \tag{6}$$

Figure 12 shows the results of this calculation, along with several others. One of these is a variational calculation of the ground state energy E_{var} of liquid ^{4}He on a cylindrical surface, by Carraro [13]. While this latter is just an upper bound to the exact energy, it probably comes within 0.2 K of the exact energy. In comparing these curves, we note that both the energy estimates E_{est} and E_{var} exhibit a common feature: there is a single total energy minimum in the vicinity of $R^*\approx 0.7$ to 0.8. We observe that $E_{est}^{(1)}$ lies significantly below Carraro's results for all values of R^*. The large discrepancy (≈ 15 K) is attributable, in our opinion, primarily to the neglect of the large increase in potential energy above the classical lattice energy $\langle V\rangle_0$. To analyze this, we make a drastic approximation: that the motion of the system is totally harmonic, i.e., a phonon description. In that case, the potential energy increase above the value $\langle V\rangle_0$ is equal to the kinetic energy per particle. This leads to a revised estimate of the energy,

$$E_{est}^{(2)}=\langle V\rangle_0+2K_{est}. \tag{7}$$

As seen in Fig. 12, the variational results lie midway between $E_{est}^{(1)}$ and $E_{est}^{(2)}$ and the minima of these functions lie close to that of the variational calculations. This comparison suggests that our model is getting the physics approximately correct. However, one must bear in mind that a more com-

plete analysis would take into account the relaxation of the system to incorporate the kinetic energy. This would be the analog of allowing the liquid density to vary in searching for the ground state, as is conventionally done in variational calculations (and was done by London with his analogous model). The result of such an approach would be a reduction in the density (as occurs for 3D ^{4}He and H_2) and in the magnitudes of all energies in the system. Such an extended analysis seems unwarranted in view of the naiveté of the present description and the availability of alternative, more accurate, computational methods.

Note added in proof. A qualitatively similar two-peak behavior of $C(T)$ was recently found by Hodak and Girifalco in simulations of C60 molecules inside large (15,15) nanotubes. The low T peak was attributed to breakup of the molecules' zigzag structure and the higher T peak to loss of longitudinal order [14].

ACKNOWLEDGMENTS

We are grateful to Carlo Carraro for a helpful discussion. This research was supported by the Petroleum Research Fund of the American Chemical Society and by Fundación Antorchas.

[1] Mary J. Bojan, M. M. Calbi, Carlo Carraro, Milton W. Cole, Silvina M. Gatica, M. L. Glasser, E. Susana Hernandez, and Milen K. Kostov, Riv. Nuovo Cimento (to be published).

[2] S.M. Gatica, G. Stan, M.M. Calbi, J.K. Johnson, and M.W. Cole, J. Low Temp. Phys. **120**, 337 (2000).

[3] D. Green and C. Chamon, Phys. Rev. Lett. **85**, 4128 (2000).

[4] F. Millot, Y. Larher, and C. Tessier, J. Chem. Phys. **76**, 3327 (1982); V. L. Pokrovsky and A. L. Talapov, *Theory of Incommensurate Crystals* (Harwood Academic Publishers, London, 1984).

[5] See, for example, A.C. Dillon and M.J. Heben, Appl. Phys. A: Mater. Sci. Process. **72**, 133 (2001); V.V. Simonyan, J.K. Johnson, A. Kuznetsova, and J.T. Yates, J. Chem. Phys. **114**, 4180 (2001); M.M. Calbi, M.W. Cole, S.M. Gatica, Mary J. Bojan, and George Stan, Rev. Mod. Phys. **73**, 857 (2001), and references therein.

[6] M.K. Kostov, M.W. Cole, J.C. Lewis, P. Diep, and J.K. Johnson, Chem. Phys. Lett. **332**, 26 (2000).

[7] J.J. Thomson, Philos. Mag. **7**, 237 (1904).

[8] A. Perez-Garrido and M.A. Moore, Phys. Rev. B **60**, 15 628 (1999); M.J. Bowick, D.R. Nelson, and A. Travesset, Phys. Rev. B **62**, 8738 (2000).

[9] To be specific, in the case $\nu=4$, the nearest neighbor separations r^* for the smaller R^* minimum are 1.11 for atoms in the same ring and 1.10 for atoms in adjacent rings (compared to the equilibrium value $2^{1/6}\approx 1.12$). For the larger R^* case, the atoms in the same ring are separated by 1.77 while those in adjacent rings are separated by 1.11.

[10] L. W. Bruch, M. W. Cole, and E. Zaremba, *Physical Adsorption: Forces and Phenomena* (Oxford University Press, New York, 1997).

[11] M.K. Balasubramanya and M.W. Roth, Phys. Rev. B **63**, 205425 (2001); M.W. Roth and M.K. Balasubramanya, *ibid.* **62**, 17 043 (2000).

[12] F. London, *Superfluids* (Dover, New York, 1954), Vol. II.

[13] C. Carraro (unpublished).

[14] See M. Hodak, Ph.D. thesis, University of Pennsylvania, 2002 (unpublished).